Inverse analytical measurement of size-independent fracture energy of Portland pozzolanic cement concrete incorporating cassava flour

Marwa Gumma Omer Adam[1*], David. O. Koteng[2], Joseph Ng'ang'a Thuo[3], Mohammed Matallah[4]

[1]Civil Engineering Department, Institute for Basic Science, Technology and Innovation, Pan African University Hosted at Jomo Kenyatta University of Agriculture and Technology, PO Box 62000-00200 Nairobi, Kenya.

[2] School of Civil & Resource Engineering, the Technical University of Kenya, Nairobi, Kenya.

[3]Center for Geotechnical Engineering, Department of Civil Engineering, Dedan Kimathi University of Technology, Nyeri, Kenya

[4] University of Tlemcen, Tlemcen, Kenya

marwagummaomer88@gmail.com gumma.marwa@students.jkuat.ac.ke (Marwa .G. O. Adam)

Abstract: This article provides a description of the fracture energy characteristics analysis of Portland pozzolanic cement concrete containing cassava flour with different percentages (1, 2, 3, 4, and 5%) at 90 days of curing. For notch-beamed structures, three-point bending examinations are conducted of Portland pozzolanic concrete blended cassava flour to get the force-crack mouth open movement (CMOM) graphs. Additionally, the behaviour of the slope of force movement, elements influencing the fracture energy, and the specimen breaking way are described. Finite numerical simulation analysis is the approach used to execute an inverse analysis process to determine the fracture energy evolution's trend. A nonlinear inverse analysis algorithm is implemented, and a model for minimizing damages is used to characterize the softening behaviour. Because the softened deformation mode that was used didn't take bounding impacts into account, most of the force-CMOM charts had to be changed. As a result, a reliable estimate of size-independent fracture energy of the Portland pozzolanic cement concrete containing cassava flour is achieved. The empirical observations test and the inverse analysis show that he fracture energy and further attributes of the Portland pozzolanic cement concrete incorporating cassava flour for cracking have been going up.

Key words
Fracture energy, Cassava flour, Softening behaviour, Damage model, Inverse analysis

1. Introduction

Concrete is a durable material, however, cracks can develop and propagate in it over time due to a number of reasons, such as thermal expansion, shrinkage, and shoddy building techniques [1], [2], [3], [4]. Additionally, inadequate curing and heavier loads placed on concrete elements may cause cracking by weakening and reducing their durability [5], [6], [7], [8]. Portland pozzolanic cement is an eco-friendly cement composed of a combination of Portland cement and natural pozzolana, which is a silica-based material usually made from a combination of volcanic ash and clay [9], [10], [11], [12]. Pozzolana helps to improve the quality of the cement by increasing its strength, durability, and workability. It is also resistant to shrinkage and cracking. This type of cement is also known for its low environmental impact due to its low water content and the fact that it requires less energy to produce [13], [14], [15].

The strength and durability of concrete structures can be significantly impacted by tensile stress [16], [17], [18], [19] . Under tensile stress, concrete is subject to cracking, spalling, and other forms of damaging stress. This damage may lower the concrete structure's ability to support its own weight, possibly causing it to collapse. Furthermore, tensile stress can result in micro-cracking, which can reduce concrete's permeability and increase water absorption, further weakening the concrete structure [20], [21], [22], [23]. Fracture mechanics is the one technique that relies on comprehending how cracks grow and spread on concrete [24], [25] . Because concrete has different properties due to the admixtures added (pozzolanas, fibers, cassava flour, etc.), curing conditions, porosity, manufacturing process, water-to-cement ratio, maximum aggregate size, etc., the time and amount of load needed for crack extension will be different for each type of concrete [26], [27], [28], [29].

Fracture energy is the amount of energy needed for a crack to make adjustments to the region of a broken edge and grow from an unloaded state at the start to a stage where it completely breaks apart [30], [31], [32], [33]. It serves as a gauge for the quantity of energy needed to cause a material fracture and is typically based on the region below the stress-strain curve, which is calculated by dividing the area by the thickness of the specimen [34], [35], [36]. The energy dissipation characteristic of softening the branch of the stress-strain curve is governed by fracture energy (GF), which is considered an important variable in concrete fracture characteristics. Size and ligament effect have an influence on the specific fracture energy [34], [37], [38], [39], [40]. Many of the authors who used cassava flour as a substitute material in concrete calculated the flexural strength of concrete beams directly according to the bending at three points test without addressing the use of computational modeling [41], [42], [43], [44], [45],[46].

Numerical modeling is a useful tool for evaluating the behaviour of materials under various conditions. By using numerical modeling, it is possible to determine the fracture energy for a given material and identify how this energy varies as a function of stress, temperature, and other parameters. This information is crucial for researchers and engineers looking to develop better products and materials. Numerical modeling can also help find any flaws or weaknesses in a material before it is used in an application. Renuion international laboratories and experts in construction materials-recommended Dealing with fractures is still the most widely used method for determining the concrete's particular cracking energy using samples of notched three-point bending of various dimensions and ratios of notch to depth [35]. In accordance with the RILEM's recommendations, the fracture energy can either be indirectly determined through numerical inverse analysis or directly from the load-displacement curves. Repeated numerical simulations are used in inverse analysis to approximate experimental results.

Tetra-linear [47], multilinear [48], or bilinear curves [49] may be used to approximate the softening curve. The fracture energy as determined by the load-displacement (P-d) curve was presented by RILEM and written as

$$G_f = \frac{1}{b(W-a)} \int P\partial\partial \qquad (1)$$

Where: (a) the crack's length, (W) breadth of the specimen in the direction of the crack, and (b) its thickness are all given. according to the hypothetical crack model created by Hillerborg's, energy definition intended towards providing an invariant variable (Gf) to represent the region underneath the tension-softness curve that was thought to be unique. It is generally recognized that the size effect on the RILEM GF does exist, though. Even if the specimen size (W) remains constant, G_f is still influenced by the length of the fracture (a). PCMOD curves search for the (r-dw) graph displaying the energy of breaking when using inverse analysis. If the inverse analysis is performed with a model that ignores boundary effects, our recommendation is to only include a part of the P-d curves where it is anticipated that the variance of the current fracture energy would be homogeneous. In this area (the inner zone), it is possible to get an excellent estimate of the size-independent fracture energy (GF).

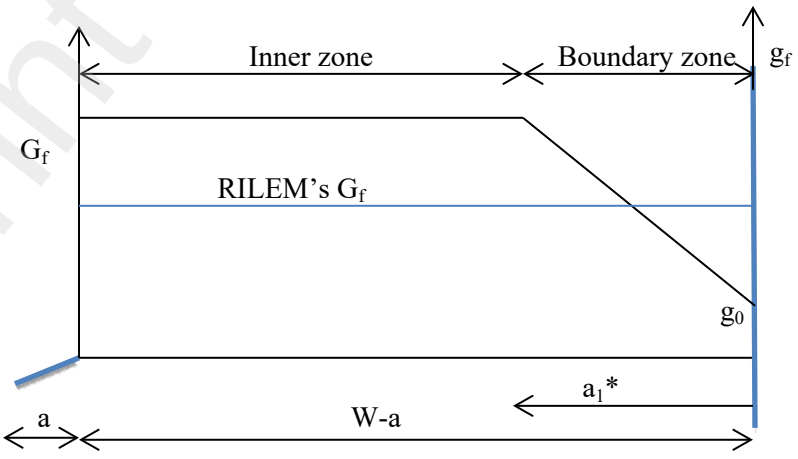

Fig 1. Fracture energy model distribution

A careful review of the literature reveals that there aren't many works that use an inverse analysis method to simulate the stress-strain curves of Portland pozzolanic cement concrete using cassava flour. The aim of this study is to simulate the stress-strain behaviour of HSC to determine the influence of cassava flour by mixing a proportioned admixture with Portland pozzolanic cement as an additive, on the fracture properties of high-strength concrete. On rectangular notched beam specimens aged 90 days; three-point bending tests are carried out experimentally. The Load-CMOD Shapes are generated. The softening behaviour of PPCC containing CF is represented using a damage-based model to be able to calculate the size-independent fracture energy. Due to the irregular nature of the softening, the opposite approach is conducted using the Levenberg-Marquardt algorithm. To calculate a fracture energy that is independent of size, exclusively a portion of the load-CMOM curves is fitted. There was no research on cassava flour's impact under these usage circumstances.

2. Fundamentals of modeling

2.1. damage-model isotropy

An isotropic damage-based model is a specific kind of substance system used to describe the behaviour of materials that experience damage or failure. This model is based on the idea that the material has a homogeneous microstructure and is isotropic, which means that its mechanical properties are the same in all directions [50], [51], [52]. The mechanical behaviour of materials experiencing progressive damage under loading is predicted using models based on isotropic damage. These models are based on the idea that damage to a material is caused by the buildup of tiny holes or cracks in the material, which makes the material less stiff and strong. The linear elastic damage model is the most basic type of isotropic damage-based model [53], [54]. This model supposes, given that it contains data, that the component responds linearly and elastically up to a certain point of injury, after which it behaves nonlinearly. The difference between the material's original and current stiffness is known as the damage variable, abbreviated as D [55], [56], [57]. The substance becomes less stiff as damage builds up, and the damage variable rises. When damage models are used, the softening damage curve describes the softening of the stress-crack opening curve. A factor affecting destruction that describes the cracking technique is used to account for the connection between tensile softening and fracture. Smeared is the best way to describe the component's performance in the brokenness processing location, and a weakened region is used to represent the area where the fracture occurs.

Following formulae control the linear elastic damage model:

$$\delta = (1 - D) \times E \times \varepsilon \quad (2)$$

$$D = 1 - \mathrm{Exp}\,(-K \times \varepsilon) \quad (3)$$

Where *E* young factor of materials, ε is strain, and K damage constant. The equation (2) relates stress to strain for a linear elastic material. The third one defines the relationship between the strain and the damage variables. The damage constant, K, is a material property that relates the strain to the accumulation of damage in the material.

A damage evolution rule can be incorporated into the linear elastic damage model to expand it to cover nonlinear behaviour. According to the damage evolution law, the damage variable adjusts to a growing load and damage accumulation. The exponential damage law, which is denoted by the following, is one widely used damage development law.

$$D = 1 - \exp\left[-k \times \sqrt{\sqrt{(\delta_{ij} - \delta 0_{ij})}} \times d\varepsilon_{ij}\right] \quad (4)$$

Where δ_{ij} force magnitude, δ_{0ij} initial yield force magnitude, $\sqrt{\sqrt{(\delta_{ij} - \delta 0_{ij})}} \times d\varepsilon_{ij}$ is the plastic strain
The positive eigenvalues of the strain tensor are used to calculate the corresponding strain

$$\varepsilon^{-} = \sqrt{(\varepsilon_1^2)} + (\varepsilon_2^2) + (\varepsilon_3^2) \quad (5)$$

If the deformation is homogeneous, the evaluation of the damaged area is determined using
$d_\varepsilon \geq 0$

$$d_d = \left[\frac{\varepsilon^{-} d0(1 + B\varepsilon^{-})}{\varepsilon^{-2}}\right] \quad (6)$$

When $d\varepsilon = d\varepsilon^{-}$, and $dd = 0$, $d\varepsilon = 0$
The total damage assessment value is

$$d = 1 - \frac{\varepsilon d0}{\varepsilon} \exp\left(B(\varepsilon do - \varepsilon^{-})\right) d > 0 \quad (7)$$

2.2. One-D analysis using the energy normalization

In one-dimensional analysis models, energetic regularization is a method that can be used to simplify the model while also improving the stability and accuracy of the data representation. By adding a penalty word to the model's cost function, energetic regularization seeks to improve performance. This penalty term is intended to deter the model from over fitting the data by penalizing any departure from the "mean" or average values of the data elements. When this penalty term is included, the model is more likely to discover a solution that best fits the entire set of data rather than just the data points with the highest values. In energetic regularization, the penalty term is usually given as a parameter that can be changed depending on the model's level of complexity. The model is permitted to become more complex as the penalty term's value increases. This keeps the model stable while allowing it to capture more of the underlying structure of the data. To force the identical energy loss regardless of component dimension, Modifying the tension-weakening characteristic is necessary.

$$\frac{G_f}{h} = \int_0^{\infty} ((1-d)E_\varepsilon)\, d_\varepsilon \quad (8)$$

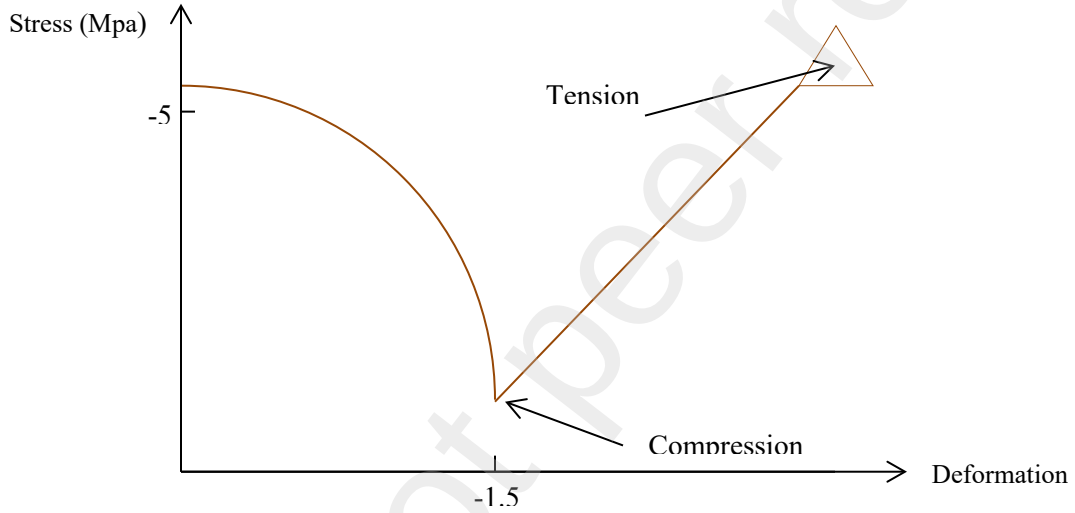

Fig. 2 a single-axis compression-tension reaction

Where h is the standard gauge or the area where damage is growing that must be connected to the fracture zone's breadth. $h = \sqrt{A_{element}}$, where $A_{element}$ is the finite element zone. $g_{f\,element}$, is the location of the breaking force is considered becoming distributed uniformly across finite components in each element. $G_{f\,element} = h \times g_{f\,element}$.

The total fracture energy can present by:

$$\frac{G_f}{h} = \int_o^{\varepsilon do} (YM.\partial) d\partial + \int_{\partial_{d0}}^{\infty} \left(\frac{\varepsilon d_0}{\partial} \text{exponential } [B(\varepsilon do - \partial])\, E\varepsilon d\varepsilon \quad (9)$$

$$\frac{G_f}{h} = \frac{f_t \varepsilon d_0}{2} + \frac{f_t}{B} \quad (10)$$

$$B = \frac{ft}{\frac{Gf}{h} - \frac{ft\varepsilon d0}{2}} \quad (11)$$

Where f_t is the tensile strength, YM is the Young modulus, and B is the factor used to govern the softening curve. Figure 3. Utilizing various discretization n is the total amount of components, and n = 1-1, 2-1, and 3-1.

Load
(KN)

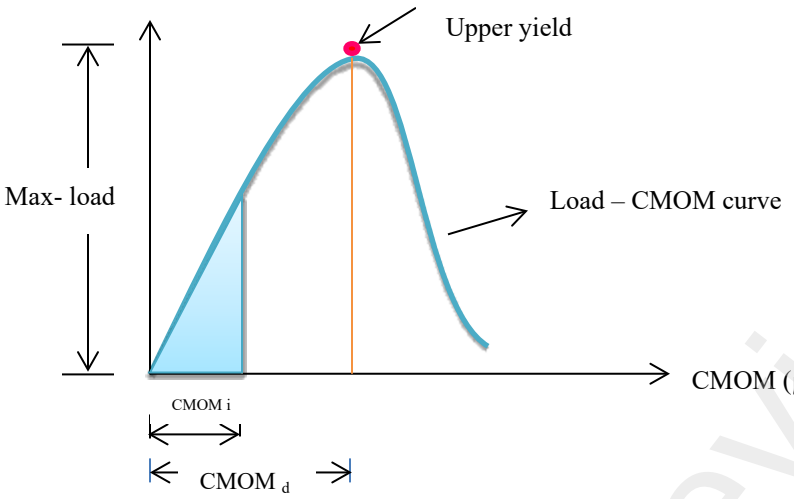

Fig. 3 Standard CMOM curve

2.3. 2D analysis using the energy normalization

This project seeks to leverage an inverse analysis technique to figure out how much energy it takes for Portland pozzolanic cement with cassava flour to break after 90 days. Three-point bending experiments are carried out. Uniaxial tension was used to assess the fracture energy equation (10). Even though the fracture is modeled, the load condition throughout the crack's course is not uniaxial for a pointed beam subjected to three-point flexion. The biaxial stress state has an impact on the energy dissipated during cracking [58]. Jirasek and Bauer assessed the two-dimensional configuration of the crack band theory in [58], [59], [60]. A straightforward damage model is used to analyse the biaxial stress impact of a 3-pin deformation test conducted on a notch beam. Similar to the shape that was empirically investigated (Figure. 7) was used for a three-point bending test on a notched beam. The damage model mentioned above is tested numerically using the fracture energy calculated for the underlying single-axis strain (Equation. 10). The goal is to assess the energy lost in the cracking zone and contrast it with the energy intake from the fracture. This particular collection of variables is taken into consideration (YM = 45 GPA, m = 0.21, f_t = 2.55 MPa, G_f = 101 N/m). Four-sided nodes with linear interpolation components make up the beam's grid (Fig. 4). The area of the finite element in the middle of the beam is approximately 1.6 mm. Equation is used to calculate the value of B. Eq (11). The comprehensive excitement of the beam is depicted in Fig. 4 (load vs. deflection). These evolutions are calculated for the finite element that first cracks in the front of the crevice. Diagrams of principle stresses versus principal strains are shown in Fig. 6. Maximum fracture energy is equal to:-

$$G_f = h \times \left(\int_0^{\infty} \delta 1 d\varepsilon 1 + \int_0^{\infty} \delta 2 d\varepsilon 2 \right) = 103 N/M \qquad (12)$$

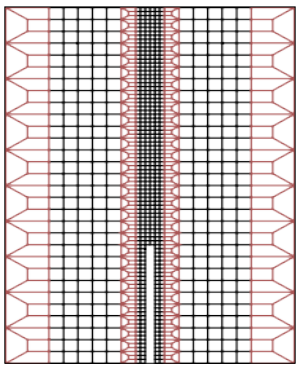
Notch

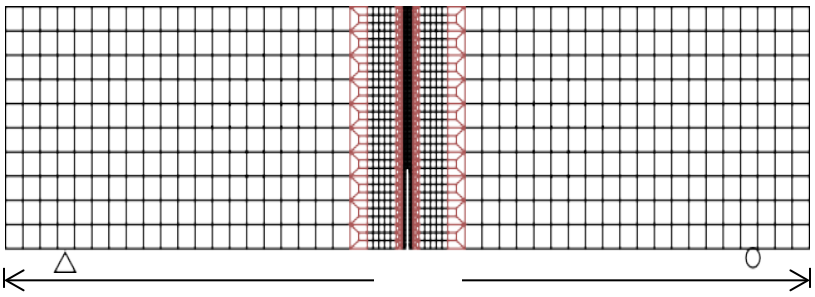

Fig. 4 concrete beam structure lattice

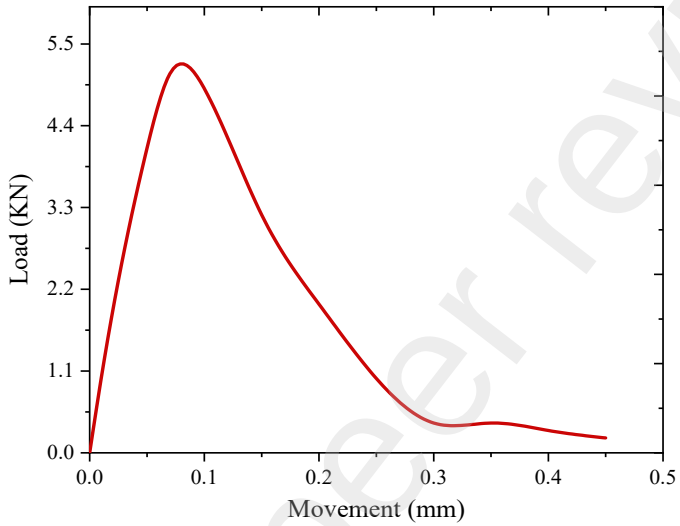

Fig. 5 the mathematical load-movement graph

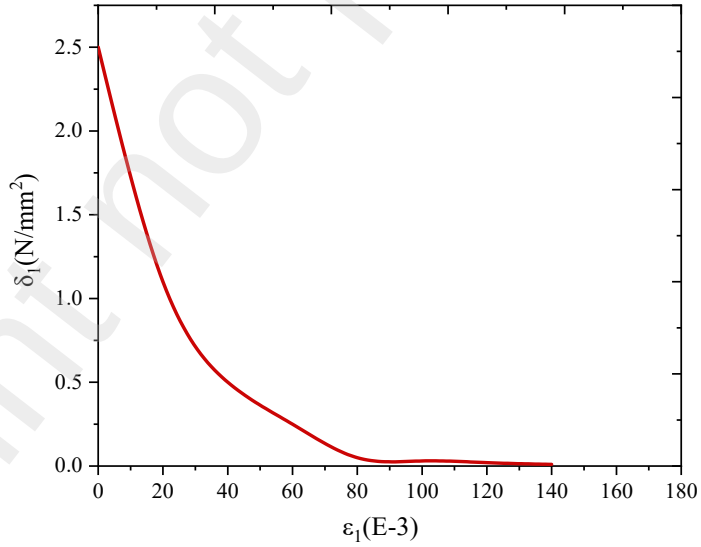

Fig. 6 principle stress – principal strain

3. Inverse analysis method

It is assumed that all finite elements have constant fracturing force; this is the region beneath the stress-displacement softness graph. Through the use of inverse analysis and the damage model, it is possible to determine a trend in the age development of Portland pozzolanic cement concrete fracture energy. Tensile strength and fracture energy are considered to be the basic input material characteristics. As a result of the transition length a1's restriction (Fig. 1), Just the interior region might be used to apply the template, where it was possible to calculate the size-independent fracture energy. Two-

linear distribution is thought to describe the energy difference along the opening pathway in accordance with the local energy concept, taking the boundary impact into consideration. The transition length could be calculated when the P-d lines for samples of varying dimensions were used to provide the energy of fracture in the RILEM. The impact of the threshold amount on the determined fracture force should be examined; two distinct CMOD values are taken into account. Therefore, when performing inverse analysis, measuring the size-independent energies of fractures requires just portion fitting of the P-CMOM slope. Next to the maximum point force, the P-CMOD curve's lengthy tail is ignored.

3.1 Analysis algorithm

DLSA algorithm, a notable example of significant techniques with the purpose of resolving multiple non-linear problem sets, used to do inverse analysis. It is based on an iterative method to find a multivariate function's minimum that is defined as the form of the total square of quadratic actual value variables [61]. The weighted sum of the squared inaccuracies in the observed information D (ui) as well as the curve-fit function D (ui, p), whereas V is a matrix representing the deformation model's variables (V = f_t, G_f), must be minimized in order to find the best solution for graph of P-CMOM experimental.

DLSA nonlinear equation is presented by

$$[ZJ^T + I\lambda]\alpha = ZJ^T(D - D^*) \qquad (13)$$

J presented jacobian matrix. Z the measuring matrix with $Z_{ii} = 1/Z_{ii}$. Backward differences are used to quantitatively estimate the Jacobian matrix in each iteration. The study uses the answer obtained for every stage, like an input factor for the following step.

Table 1
Properties of aggregates

	Coarse aggregate	Fine aggregate
Density	1.54	1.68
Water absorption	3.50	3.86
Water content (%)	1.8	2.9

4. Trial

4.1. Specific concrete composition

The materials of the concrete mix are composed of an aggregate, such as gravel, sand, cassava flour, Sika Viscoflow-615 KE Superplasticizer, and PPC as a glue binder to hold the aggregate together in a solid mass. In the control mixture, designated by CM, there was 0% cassava flour. The remaining five mixtures were created by varying the percentages of CF added to PPC for each of the other five mixtures: 1, 2, 3, 4, and 5%. All of the specifications for the concrete mixture containing cassava flour are displayed in the table below.

Table 2
Concrete mixture proportion

Mix	C.A			F.A	Cement	Water	w/b ratio	S.P	C.F (%)	C.F
	6.35-12.7	3.18-6.35	1.58-3.18							
M-0	406	539	53.00	531	501	171	0.350	4.0	0.00	0.00
M-1	406	539	53.00	531	501	171	0.350	4.040	1.00	5.00
M-2	406	539	53.00	531	501	171	0.350	4.080	2.00	10.00
M-3	406	539	53.00	531	501	171	0.400	4.120	3.00	15.00
M-4	406	539	53.00	531	501	171	0.400	4.160	4.00	20.00
M-5	406	539	53.00	531	501	171	0.400	4.200	5.00	25.00

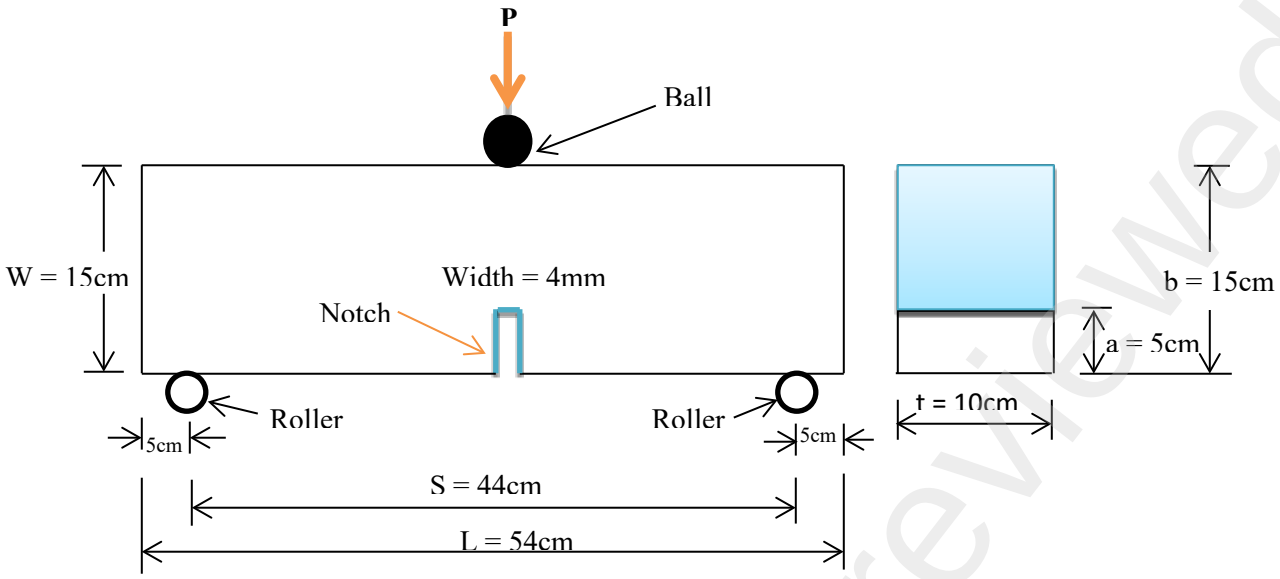

Fig.7 Illustration regarding the tribal-pint deformation testing setup diagrams

4.2 Experiment technique

Molds measuring 54 * 15 * 15 cm^3 were used to pour concrete (see Fig. 7). The position of the notch was determined before casting by inserting a wooden slat with a thickness of approximately 4 mm. After 24 hours, the formwork and a wooden slat were removed from the concrete, which contained cassava flour and Portland pozzolanic cement. It takes 90 days for the samples to cure in the water. When testing the samples, the reflector was used to quantify the deflection. We used a 150 kN-capacity universal testing machine. The beam and the load jack were separated by a piece of wood. At the sluggish speed of 0.50 µm/s, all experiments were conducted while controlling the crack mouth opening displacement. As a result, it took only approximately a minute to reach the peak load. With the use of these tests, the load's relationship to timing, CMOM, and bending was discovered. Although the force-CMOD is usually adequate, sometimes the load-deflection curve is not as accurate. Data was gathered every single instant.

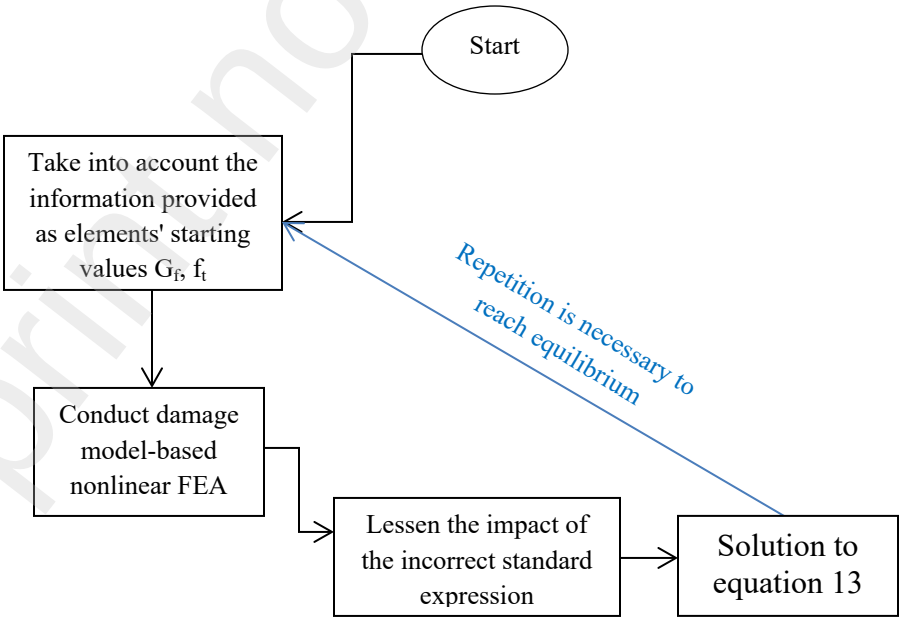

Fig. 8 a method based on mathematics

Fig. 9 CMOM testing process

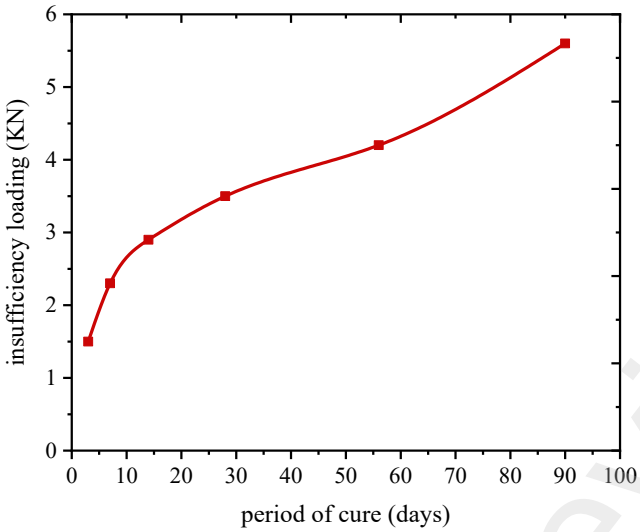

Fig. 10 evolving breakdown loads

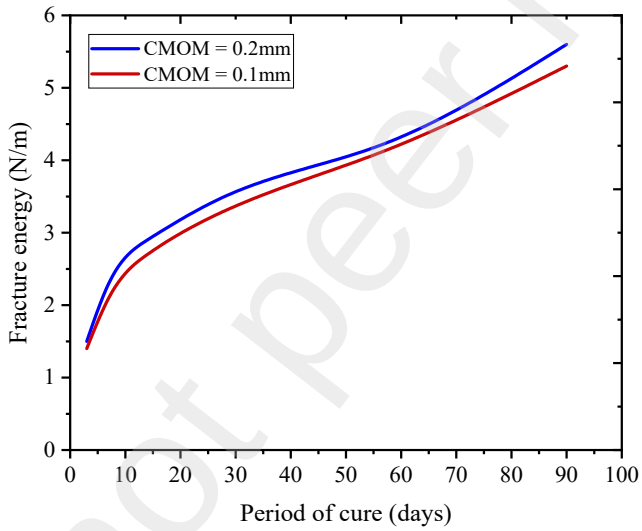

Fig. 11 Age-related changes in the size independent of fracture energy (CMOM = 0.20mm, CMOM = 0.10mm)

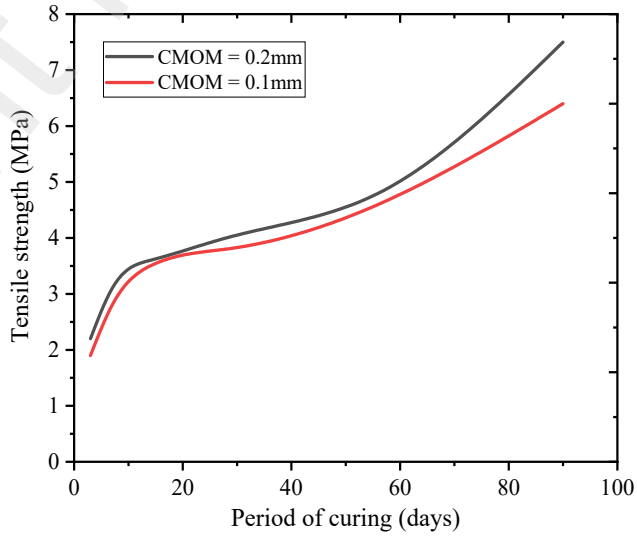

Fig. 12 evaluation of the tensile strength with the age (CMOM = 0.2mm, CMOM = 0.1mm)

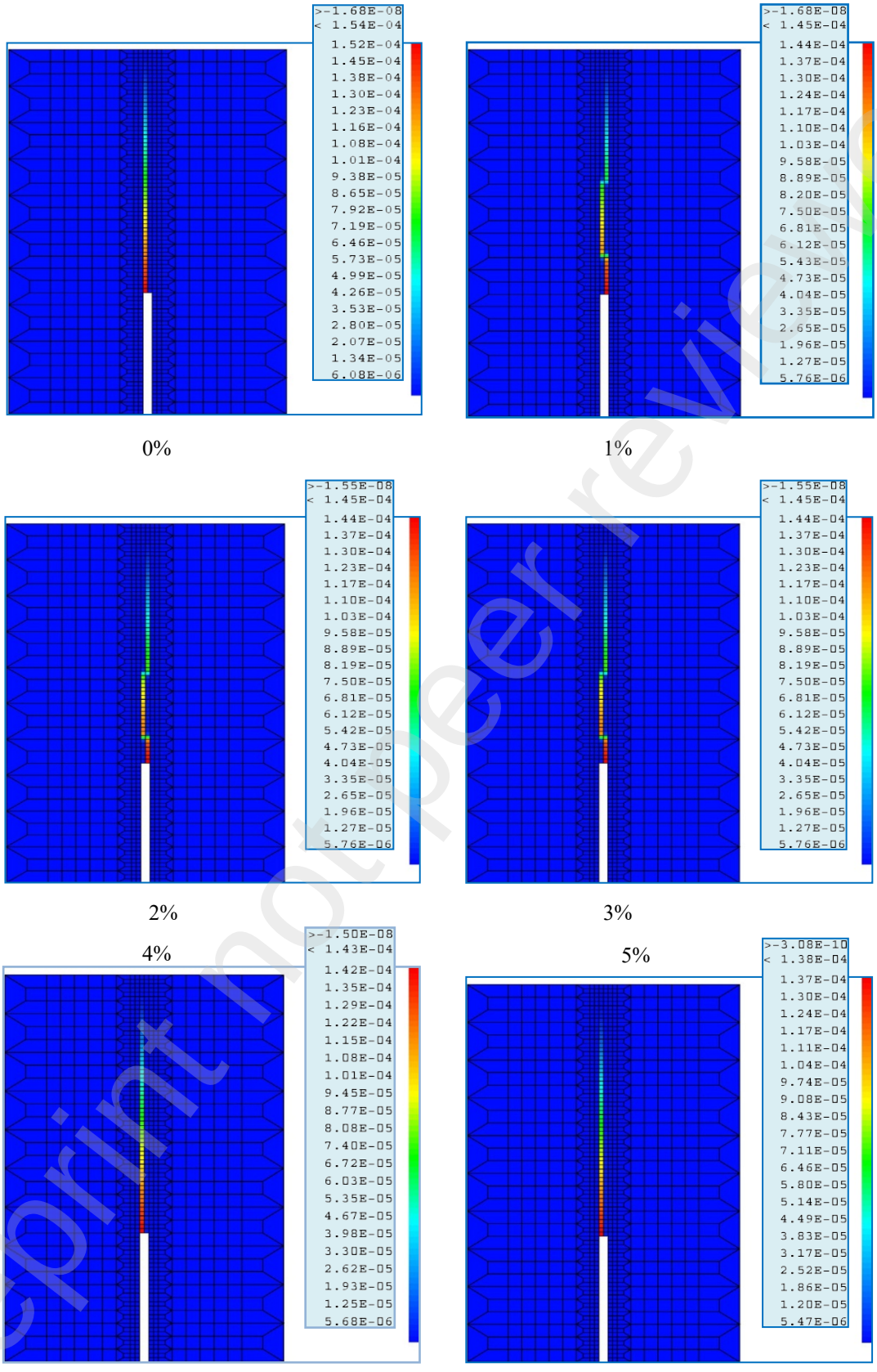

Fig. 13 breaking down regions for PPCC with CF at various amounts of cassava flour

5. Results and discussion

5.1 Findings from the testing

The elasticity of concrete mixes made with various amounts of cassava flour can be measured using the CMOM curve analysis for Portland pozzolanic cement using cassava flour. The best amount of cassava flour to use to create concrete with the necessary strength and durability is calculated using this method. The compression force necessary to deform a concrete sample of a specific size is measured for the CMOM curve analysis. The amount of cassava flour in the sample is then plotted against the force. The P-CMOM curves for the Portland pozzolanic cement concrete incorporating cassava flour were thoroughly examined. According to the chart in Fig. 15, the elastic part's failure load and slope both rise through time, even though the yield area portion falls off quickly. The rise in elasticity and a breakdown force indicates that the fracture qualities of PPC concrete with cassava flour improved over time. The progression of the YM over time probably applied to explain the rise in elastic slope. Figure 16 illustrates the failure vs. curing times and provides insight into the progression of the strength of pozzolanic cement concrete with C.F. This load was minimal at an early age and later significantly increased. When compared to those obtained for control, it reached 5.7 KN at the age of 90 days. Because of the hydrated conditions, it can be interpreted as having evolved to its later phases and the cohesiveness between the various components has grown stronger after 14 days.

5.2 Findings from simulation

Fig. 8 is a method based on mathematics using the FEAM cast3M code. The broken energy estimate discovered under uniaxial tension conditions is used in the inverse analysis approach (Equation.7) For an experiment with an age of 90 days, the best-fitting variable setting is discovered. Through its highest yield point force, the compound appears to behave nonlinearly. It is now at its strongest point. The deformation model utilized in this study assumes that the regional characteristics are flexible-linear until the maximum yield, although this might not have been accurate during the early curing stages (7–14 days), whenever the material appears to have both viscosity and flexible properties. This may help figure out whether the experimental information and the estimated numerical findings diverge slightly in this part of the study. Since the fracture energy is expected to be constant over the element size, as stated in the introduction, the damage model used to carry out the inverse analysis is unable to account for the border influence. The suggested remedy involved fitting only a section of the P-CMOM curves. This leads to the estimate of the size-independent fracture energy. The growth of the size-independent fracture energy with age is depicted in Fig. 11. Ultimately, the statistics show an "upward trend," which is consistent with the findings of the experiment. The development of the tensile strength is seen in Fig. 12. A rising trend is seen in terms of fracture energy. The size-independent fracture energy could be calculated in the inner zone prior to the break reaching the back barrier, according to the local energy concept. Figure 13 illustrates the crack-opening fields for various ages. According to the break geometries observed on all supports, the crack does not exceed the border limit, and the fracture process is not significantly impacted by boundary effects at the movement limit used to do inverse analysis.

Conclusion

The article examines the fracture properties of concrete made with Portland pozzolanic cement and cassava flour after 90 days of curing. 3-pint deformations were conducted experimentally on concrete samples with pointed supports at 90 days. The P-CMOM charts that were obtained show an upward tendency in the progression of yield point weakening and collapse force provides a broad picture of the performance of the Portland cement concrete. A softening deformation theory and a nonlinear inverse analysis method have been used to build an inverse analysis procedure to analyse the evolution of the fractured concrete features. The input variables have been used for two fundamental fracture criteria. As a whole, the numerical findings point to an "upward pattern" in the fracture's properties. A little section from the δ-CMOM lines considering that the deformation model used to perform the inverse analysis anticipates a constant relationship along the fracture measurement, fitting techniques were applied. However, the bilinear model has produced a decent estimate of the size-independent fracture energy.

Authorship Statement

Marwa Gumma Omer Adam: Conceptualization, Methodology, Validation, Formal analysis, Investigation, Resources, Writing – original draft, Visualization. David Otieno Koteng: Writing – Review & editing, Supervision. Joseph Ng'ang'a Thuo: Writing – Review & editing, Supervision. Mohammed Matallah: Writing – review & editing, Supervision.

References

[1] P. Nama, A. Jain, R. Srivastava, and Y. Bhatia, "Study on Causes of Cracks & its Preventive Measures in Concrete Structures," *J. Eng. Res. Appl. www.ijera.com*, vol. 5, no. 2, pp. 119–123, 2015, [Online]. Available: www.ijera.com.

[2] C. J. Chitte, "Study on Causes and Prevention of Cracks in Building," *Int. J. Res. Appl. Sci. Eng. Technol.*, vol. 6, no. 3, pp. 453–461, 2018, doi: 10.22214/ijraset.2018.3073.

[3] M. Safiuddin, A. B. M. A. Kaish, C. O. Woon, and S. N. Raman, "Early-age cracking in concrete: Causes, consequences, remedialmeasures, and recommendations," *Appl. Sci.*, vol. 8, no. 10, 2018, doi: 10.3390/app8101730.

[4] J. Xin *et al.*, "Evaluation of early-age thermal cracking resistance of high w/b, high volume fly ash (HVFA) concrete using temperature stress testing machine," *Case Stud. Constr. Mater.*, vol. 16, no. November 2021, p. e00825, 2022, doi: 10.1016/j.cscm.2021.e00825.

[5] M. Flah, A. R. Suleiman, and M. L. Nehdi, "Classification and quantification of cracks in concrete structures using deep learning image-based techniques," *Cem. Concr. Compos.*, vol. 114, no. January, p. 103781, 2020, doi: 10.1016/j.cemconcomp.2020.103781.

[6] L. Mengel, H. W. Krauss, and D. Lowke, "Water transport through cracks in plain and reinforced concrete – Influencing factors and open questions," *Constr. Build. Mater.*, vol. 254, p. 118990, 2020, doi: 10.1016/j.conbuildmat.2020.118990.

[7] Q. Zhang, K. Barri, S. K. Babanajad, and A. H. Alavi, "Real-Time Detection of Cracks on Concrete Bridge Decks Using Deep Learning in the Frequency Domain," *Engineering*, vol. 7, no. 12, pp. 1786–1796, 2021, doi: 10.1016/j.eng.2020.07.026.

[8] P. jo Chun, S. Izumi, and T. Yamane, "Automatic detection method of cracks from concrete surface imagery using two-step light gradient boosting machine," *Comput. Civ. Infrastruct. Eng.*, vol. 36, no. 1, pp. 61–72, 2021, doi: 10.1111/mice.12564.

[9] B. Kanagaraj, E. Lubloy, N. Anand, V. Hlavicka, and T. Kiran, "Investigation of physical , chemical , mechanical , and microstructural properties of cement-less concrete – state-of-the-art review," *Constr. Build. Mater.*, vol. 365, no. December 2022, p. 130020, 2023, doi: 10.1016/j.conbuildmat.2022.130020.

[10] M. Tailing *et al.*, "Study of Geopolymer Composites Based on Volcanic Ash , Fly," 2022.

[11] R. Article *et al.*, "Comprehensive review of the properties of fl y ash - based geopolymer with additive of nano - SiO 2," pp. 1478–1498, 2022.

[12] M. E. Kalaw, J. M. Adiarte, R. Cruz, K. Mae, C. A. Vega, and M. A. Promentilla, "Strength and fire resistance characteristics of geopolymers synthesized from volcanic ash , red clay and waste pen shells Strength and fire resistance characteristics of geopolymers synthesized from volcanic ash , red clay and waste pen shells," 2021, doi: 10.1088/1757-899X/1109/1/012068.

[13] J. D. Waghmare, S. S. Patil, S. M. Patil, and M. Maske, "Study and Review of Properties and Applications of Portland Pozzolana Cement," *ASEAN J. Sci. Eng.*, vol. 1, no. 1, pp. 13–18, 2021, doi: 10.17509/ajse.v1i1.37980.

[14] M. Science, "COMPARISON OF CORROSION BEHAVIOR OF STEEL REINFORCEMENT BARS IN ORDINARY PORTLAND CEMENT AND PORTLAND POZZOLANA CEMENT ENVIRONMENTS COMPARISON OF CORROSION BEHAVIOR OF STEEL REINFORCEMENT BARS IN ORDINARY PORTLAND CEMENT AND PORTLAND POZZOLANA CEMENT," no. April, 2022.

[15] A. Derakhshani, A. Ghadi, and S. E. Vahdat, "Study of the effect of calcium nitrate, calcium formate, triethanolamine, and triisopropanolamine on compressive strength of Portland-pozzolana cement," *Case Stud. Constr. Mater.*, vol. 18, no. December 2022, p. e01799, 2023, doi: 10.1016/j.cscm.2022.e01799.

[16] S. M. Anas *et al.*, "Damage response of conventionally reinforced two-way spanning concrete slab under eccentric impacting drop weight loading," *Def. Technol.*, vol. 19, pp. 12–34, 2023, doi: 10.1016/j.dt.2022.04.011.

[17] J. Miah *et al.*, "Impact of external biaxial compressive loading on the fire spalling behavior of normal-strength concrete To cite this version : HAL Id : hal-04007428 Impact of external biaxial compressive loading on the fire spalling behavior of normal-strength concrete ," 2023.

[18] M. Yıldırım and H. B. Özhan, "Residual Durability Performance of Glass Fiber Reinforced Concrete Damaged by Compressive Stress Loads," pp. 1–10, 2023.

[19] F. Althoey *et al.*, "Case Studies in Construction Materials Physical , strength , durability and microstructural analysis of self-healing concrete : A systematic review," *Case Stud. Constr. Mater.*, vol. 18, no. September 2022, p. e01730, 2023, doi: 10.1016/j.cscm.2022.e01730.

[20] M. M. Moein, A. Saradar, K. Rahmati, Y. Rezakhani, and P. Branch, "Reliability analysis and experimental investigation of impact resistance of concrete reinforced with polyolefin fiber in different shapes , lengths , and doses Reliability analysis and experimental investigation of impact resistance of concrete reinforced," no. March, 2023, doi: 10.1016/j.jobe.2023.106262.

[21] C. Lv and J. Liu, "Alkaline Degradation of Plant Fiber Reinforcements in," 2023.

[22] X. Gao, L. Zhou, X. Ren, and J. Li, "Rate effect on the stress–strain behavior of concrete under uniaxial tensile stress," *Struct. Concr.*, vol. 22, no. S1, pp. E815–E830, 2021, doi: 10.1002/suco.201900567.

[23] B. Hu, T. Meng, Y. Li, D. Li, and L. Chen, "Dynamic splitting tensile bond behavior of new-to-old concrete interfaces," vol. 281, pp. 12–23, 2021, doi: 10.1016/j.conbuildmat.2021.122570.

[24] J. Yao, "Tensile over-saturated cracking of Ultra-High-Strength Engineered Cementitious Composites (UHS-ECC) with artificial geopolymer aggregates," no. February, 2023, doi: 10.1016/j.cemconcomp.2022.104896.

[25] Y. Zeng, H. He, Y. Qu, X. Sun, H. Tan, and J. Zhou, "Numerical Simulation of Fatigue Cracking of Diaphragm Notch in Orthotropic Steel Deck Model," 2023.

[26] S. Khalilpour, E. Baniasad, and M. Dehestani, "Cement and Concrete Research A review on concrete fracture energy and e ff ective parameters," *Cem. Concr. Res.*, vol. 120, no. January, pp. 294–321, 2019, doi: 10.1016/j.cemconres.2019.03.013.

[27] R. Fediuk *et al.*, "Combined effect on properties and durability performance of nanomodified basalt fiber blended with bottom ash-based cement concrete: ANOVA evaluation," *J. Mater. Res. Technol.*, vol. 23, pp. 2642–2657, 2023, doi: 10.1016/j.jmrt.2023.01.179.

[28] A. Manufactured, M. Małek, and J. Kluczy, "Performance Properties of Cement – Glass Composite Bricks Polymeric Scaffolding," 2023.

[29] D. Nasr, R. Babagoli, M. Rezaei, and A. Andarz, "Evaluating the Influence of Carbon Fiber on the Mechanical Characteristics and Electrical Conductivity of Roller-Compacted Concrete Containing Waste Ceramic Aggregates Exposed to Freeze-Thaw Cycling," *Adv. Mater. Sci. Eng.*, vol. 2023, pp. 1–12, 2023, doi: 10.1155/2023/1308387.

[30] R. Long and C. Y. Hui, "Fracture toughness of hydrogels: Measurement and interpretation," *Soft Matter*, vol. 12, no. 39, pp. 8069–8086, 2016, doi: 10.1039/c6sm01694d.

[31] G. Kolesnikov, "Analysis of concrete failure on the descending branch of the load-displacement curve," *Crystals*, vol. 10, no. 10, pp. 1–12, 2020, doi: 10.3390/cryst10100921.

[32] A. Almomani, A. H. I. Mourad, S. Deveci, J. W. Wee, and B. H. Choi, "Recent advances in slow crack growth modeling of polyethylene materials," *Mater. Des.*, vol. 227, p. 111720, 2023, doi: 10.1016/j.matdes.2023.111720.

[33] H. Ruan, S. Rezaei, Y. Yang, D. Gross, and B. X. Xu, "A thermo-mechanical phase-field fracture model: Application to hot cracking simulations in additive manufacturing," *J. Mech. Phys. Solids*, vol. 172, 2023, doi: 10.1016/j.jmps.2022.105169.

[34] M. Matallah, M. Farah, F. Grondin, A. Loukili, and E. Rozière, "Size-independent fracture energy of concrete at very early ages by inverse analysis," *Eng. Fract. Mech.*, vol. 109, no. September 2021, pp. 1–16, 2013, doi: 10.1016/j.engfracmech.2013.05.016.

[35] A. R. Murthy, B. L. Karihaloo, N. R. Iyer, and B. K. R. Prasad, "Cement and Concrete Research Determination of size-independent speci fi c fracture energy of concrete mixes by two methods," *Cem. Concr. Res.*, vol. 50, pp. 19–25, 2013, doi: 10.1016/j.cemconres.2013.03.015.

[36] K. P. Vishalakshi, V. Revathi, and S. S. Reddy, "Effect of Type of Coarse Aggregate on the Strength Properties and Fracture Energy of Normal and High Strength Concrete," *Eng. Fract. Mech.*, 2018, doi: 10.1016/j.engfracmech.2018.02.029.

[37] I. M. Nikbin and H. Ahmadi, "Fracture behaviour of concrete containing waste tire and waste polyethylene terephthalate: An sustainable fracture design," *Constr. Build. Mater.*, vol. 261, p. 119960, 2020, doi: 10.1016/j.conbuildmat.2020.119960.

[38] Y. Wang, S. Hu, and Z. He, "Mechanical and fracture properties of geopolymer concrete with basalt fiber using digital image correlation," *Theor. Appl. Fract. Mech.*, vol. 112, no. September 2020, p. 102909, 2021, doi:

10.1016/j.tafmec.2021.102909.

[39] T. Qin, K. Ren, Z. Liu, Y. W. Duan, and L. Wang, “Mechanical Characteristics and Energy Evolution of Sandstone Three-Point Bending Test,” *Shock Vib.*, vol. 2021, 2021, doi: 10.1155/2021/8443777.

[40] A. Abolhasani, B. Samali, M. Dehestani, and N. A. Libre, “Effect of rice husk ash on mechanical properties, fracture energy, brittleness and aging of calcium aluminate cement concrete,” *Structures*, vol. 36, no. December 2021, pp. 140–152, 2022, doi: 10.1016/j.istruc.2021.11.054.

[41] M. Gumma, O. Adam, D. O. Koteng, J. Ng, and M. Matallah, “Analysing the Effect of Cassava Flour as a Mixture on the Physical , Mechanical , and Durability Properties of High-Strength Concrete,” vol. 8, no. 12, pp. 3866–3882, 2022.

[42] D. Oluwabusayo ONI, J. Mwero, and C. Kabubo, “Experimental Investigation of the Physical and Mechanical Properties of Cassava Starch Modified Concrete,” *Open Constr. Build. Technol. J.*, vol. 13, no. 1, pp. 331–343, 2020, doi: 10.2174/1874836801913010331.

[43] O. I. Oluwole and O. M. Avwerosuoghene, “Effects of cassava starch and natural rubber as binders on the flexural and water absorption properties of recycled paper pulp based composites,” *Int. J. Eng. Technol. Innov.*, vol. 5, no. 4, pp. 255–263, 2015.

[44] J. I. Arimanwa, D. I. Bertram, M. C. Arimanwa, and A. U. Igbojiaku, “Experimental Study on the Characteristics of Concrete Containing Cassava Flour Admixture,” no. 2013, pp. 14–19, 2021, doi: 10.9790/1813-1010011419.

[45] B. Kone, J. N. Mwero, and E. K. Ronoh, “Experimental Effect of Cassava Starch and Rice Husk Ash on Physical and Mechanical Properties of Concrete,” *Int. J. Eng. Trends Technol.*, vol. 70, no. 2, pp. 343–350, 2022, doi: 10.14445/22315381/IJETT-V70I2P239.

[46] M. Gumma, O. Adam, D. O. Koteng, J. Ng, and M. Matallah, “Results in Engineering Effects of acid attack and cassava flour dosage on the interfacial transition zone thickness , durability and mechanical characteristics of high-strength (HS) concrete,” *Results Eng.*, vol. 17, no. February, p. 101001, 2023, doi: 10.1016/j.rineng.2023.101001.

[47] Z. Zhao, S. Hee, and S. P. Shah, “Cement and Concrete Research Effect of specimen size on fracture energy and softening curve of concrete : Part I . Experiments and fracture energy,” vol. 38, pp. 1049–1060, 2008, doi: 10.1016/j.cemconres.2008.03.017.

[48] N. Bretschneider, V. Slowik, B. Villmann, and V. Mechtcherine, “Boundary effect on the softening curve of concrete,” *Eng. Fract. Mech.*, vol. 78, no. 17, pp. 2896–2906, 2011, doi: 10.1016/j.engfracmech.2011.08.006.

[49] L. Østergaard, D. Lange, and H. Stang, “Early-age stress – crack opening relationships for high performance concrete,” vol. 26, pp. 563–572, 2004, doi: 10.1016/S0958-9465(03)00074-X.

[50] K. Kunze, T. Etter, J. Grässlin, and V. Shklover, “Texture, anisotropy in microstructure and mechanical properties of IN738LC alloy processed by selective laser melting (SLM),” *Mater. Sci. Eng. A*, vol. 620, pp. 213–222, 2015, doi: 10.1016/j.msea.2014.10.003.

[51] S. Li, E. Demirci, and V. V. Silberschmidt, “Variability and anisotropy of mechanical behavior of cortical bone in tension and compression,” *J. Mech. Behav. Biomed. Mater.*, vol. 21, pp. 109–120, 2013, doi: 10.1016/j.jmbbm.2013.02.021.

[52] H. K. Park *et al.*, “Efficient design of harmonic structure using an integrated hetero-deformation induced hardening model and machine learning algorithm,” *Acta Mater.*, vol. 244, no. December 2022, p. 118583, 2023, doi: 10.1016/j.actamat.2022.118583.

[53] M. Mokhtari, E. Kim, and J. Amdahl, “A non-linear viscoelastic material model with progressive damage based on microstructural evolution and phase transition in polycrystalline ice for design against ice impact,” *Int. J. Impact Eng.*, vol. 176, no. March, 2023, doi: 10.1016/j.ijimpeng.2023.104563.

[54] V. Singh, R. Larsson, R. Olsson, and E. Marklund, “A micromechanics based model for rate dependent compression loaded unidirectional composites,” *Compos. Sci. Technol.*, vol. 232, no. October 2022, p. 109821, 2023, doi: 10.1016/j.compscitech.2022.109821.

[55] E. Chebbi, L. Ben Said, B. Ayadi, and F. Dammak, “A Continuum Damage-Based Anisotropic Hyperelastic Fatigue Model for Short Glass Fiber Reinforced Polyamide 66,” 2023.

[56] E. Address, “A simplified continuum damage model for nonlinear seismic analysis of concrete arch dams using different damping algorithms,” pp. 1–32, 2023, doi: 10.22059/CEIJ.2023.342419.1837.

[57] L. Wang and Q. Lei, “Computers and Geotechnics Modelling the pre- and post-failure behaviour of faulted rock

slopes based on the particle finite element method with a damage mechanics model," *Comput. Geotech.*, vol. 153, no. October 2022, p. 105057, 2023, doi: 10.1016/j.compgeo.2022.105057.

[58] M. Jirásek and M. Bauer, "Numerical aspects of the crack band approach," *Comput. Struct.*, vol. 110–111, pp. 60–78, 2012, doi: 10.1016/j.compstruc.2012.06.006.

[59] I. Fernandez, C. G. Berrocal, and R. Rempling, "Two-dimensional strain field analysis of reinforced concrete D-regions based on distributed optical fibre sensors," *Eng. Struct.*, vol. 278, no. August 2022, p. 115562, 2023, doi: 10.1016/j.engstruct.2022.115562.

[60] M. Wei, F. Dai, Y. Liu, and R. Jiang, "A fracture model for assessing tensile mode crack growth resistance of rocks," *J. Rock Mech. Geotech. Eng.*, vol. 15, no. 2, pp. 395–411, 2023, doi: 10.1016/j.jrmge.2022.03.001.

[61] J. Kasahara, V. Korneev, and M. S. Zhdanov, "Handbook of Geophysical Exploration: Seismic Exploration: Preface," *Handb. Geophys. Explor. Seism. Explor.*, vol. 40, no. C, 2010.